Collisions of HCl, DCl, and HBr with Liquid Glycerol: Gas Uptake, D → H Exchange, and Solution Thermodynamics

Bradley R. Ringeisen,† Annabel H. Muenter, and Gilbert M. Nathanson*

Department of Chemistry, University of Wisconsin—Madison, 1101 University Avenue, Madison, Wisconsin 53706-1322

Received: October 25, 2001; In Final Form: January 30, 2002

Gas−liquid scattering, D → H exchange, and time-dependent uptake measurements are used to follow HCl, DCl, and HBr as they strike the surface of the neutral, hydrogen-bonding liquid glycerol. In this and the following paper, we report studies of gas−liquid energy transfer and trapping, the nature of HCl and HBr interfacial and bulk phase dissociation and recombination, and the thermodynamics of HCl solvation. We find that most HCl and HBr molecules readily dissipate their excess kinetic energy and thermalize at the surface of glycerol, even at impact energies up to 100 kJ mol^{-1} and glancing angles of incidence up to 60°. Nearly all thermally accommodated HBr molecules dissolve in glycerol for longer than 10 s. HCl is less acidic and dissolves reversibly for times of 0.1 to 1 s at incident HCl fluxes of (2 to 0.2) × 10^{15} cm^{-2} s^{-1}, respectively. Experiments utilizing DCl show that this reversible solvation is accompanied by dissociation into D^+ and Cl^-, $D^+ \rightarrow H^+$ exchange, and HCl desorption. The residence times of HCl in glycerol and their temperature dependences yield $\Delta G^\circ_{HCl}(gly) = -19 \pm 2$ kJ mol^{-1}, $\Delta H^\circ_{HCl}(gly) = -67 \pm 4$ kJ mol^{-1}, and $\Delta S^\circ_{HCl}(gly) = -165 \pm 20$ J mol^{-1} K^{-1} for $HCl(g) \rightleftharpoons H^+(gly) + Cl^-(gly)$ at 294 K.

Introduction

The transfer of an acidic molecule from the gas phase into solution involves passage of the molecule through the interfacial region between gas and liquid. This region absorbs the energy of impact of the gas molecule and provides the initial environment for solvation, dissociation, and recombination. For acidic gases and protic liquids, this environment changes sharply across the interface: the dissociation of HCl into H^+ and Cl^- is endothermic by 1400 kJ mol^{-1} in the gas phase but exothermic by 75 kJ mol^{-1} in bulk H_2O. Our goals are to determine where HCl dissociates and recombines as it passes through the surface of a protic liquid and to help elucidate the differences in HCl solvation and dissociation in the interfacial and bulk regions of the liquid. In this and the following paper, we use molecular beam scattering experiments to compare the fates of HCl, DCl, and HBr after they strike the surface of glycerol, a low vapor pressure, hydrogen-bonding liquid ($HOCH_2CH(OH)CH_2OH$). The experiments demonstrate that the glycerol interface is not just a gateway into the bulk liquid but a region where HCl molecules can dissociate, recombine, and desorb before diffusing deeply into the liquid, even when longtime solvation of the ions in the bulk is very favorable.

Figure 1 outlines the channels we observe for a deuterated acid molecule DX (X = Cl, Br) striking the surface of glycerol. During the gas−liquid encounter, the incident molecule may scatter directly from the surface in one or a few collisions with probability $p_{scatter}$ or fully dissipate its incident kinetic energy (thermalization) and bind momentarily to the surface with probability p_{trap}. This gas−surface trapping is followed by one of several pathways. DX molecules may desorb immediately as DX with probability $p_{trap-desorb}$. Alternatively, thermalized DX molecules may enter glycerol as intact DX or after first dissociating into D^+ and X^- in the interfacial region with a combined probability p_{solv}. We show below that all DX that enter bulk glycerol ultimately dissociate into D^+ and X^-, followed by $D^+ \rightarrow H^+$ exchange and slow recombination and desorption of HX. The experiments in the next paper also identify an immediate, interfacial DCl → HCl exchange and desorption channel with probability p_{ied}.

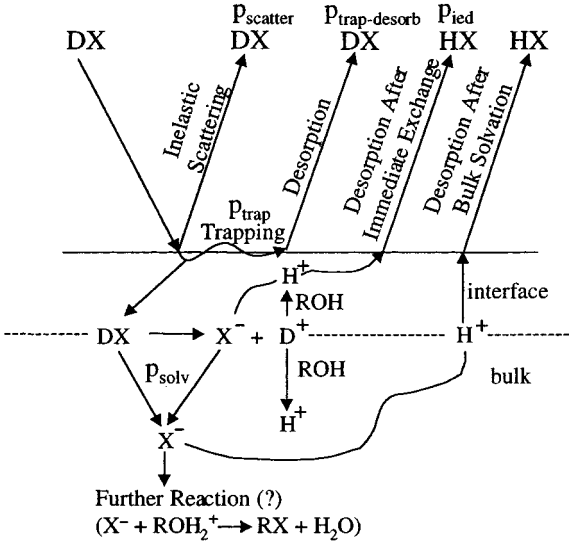

Figure 1. Observed pathways for an acidic molecule DX colliding into liquid glycerol (ROH). DX dissociation and HX recombination may occur in the interfacial or bulk regions of the liquid.

We chose glycerol because it is a low vapor pressure, protic liquid in which acids, bases, and salts ionize extensively.[1−3] It is a highly viscous solvent ($\eta = 1300$ cP at 294 K) with a large dielectric constant ($\epsilon = 41$) and a dissociation constant in water of 3 × 10^{-15} that is similar to the value for water itself.

* Corresponding author. E-mail: nathanson@chem.wisc.edu.
† Present address: Naval Research Laboratory, Washington, D.C. 20375.

10.1021/jp013960w CCC: $22.00
Published on Web 04/23/2002

Glycerol's high boiling point of 563 K and high vaporization enthalpy of 92 kJ mol^{-1} limit the vapor pressure to 1×10^{-4} Torr near room temperature.[4,5] This low volatility ensures that over 95% of the impinging HX molecules strike the glycerol surface and not glycerol vapor molecules when the liquid is placed inside a vacuum chamber.[6] Glycerol crystallizes at 291 K but readily supercools, with a glass transition temperature near 190 K.[7,8]

The initial interactions of HCl and HBr striking glycerol should be governed by the surface properties of the liquid. Molecular dynamics simulations predict that the surface of glycerol is 60% OH and 40% CH and CH_2 and that the density changes sharply across the interface, dropping from 90 to 10% over 4 Å.[9,10] Sum frequency generation studies further indicate that all OH groups at the surface are hydrogen bonded and that the carbon skeleton is roughly perpendicular to the surface plane.[11] This orientation is consistent with that determined from ion scattering measurements.[12] Despite the large surface coverage of CH and CH_2 groups, the surface tension of glycerol of 63 dyne cm^{-1} is only slightly lower than the 72 dyne cm^{-1} value for water. Glycerol's low surface entropy of 16 J mol^{-1} K^{-1} is also characteristic of strongly hydrogen-bonded liquids.[13] In previous scattering studies, we found that NH_3 and D_2O thermalize more readily than do Ne or CH_4 at the surface of glycerol, suggesting that these protic molecules interact more strongly with surface OH groups during a gas−liquid collision.[6] Computer simulations reveal that this stronger bonding occurs as the D_2O molecules tumble over the surface and reorient into favorable hydrogen-bonding configurations.[9,10] The high reaction probabilities measured below suggest that HCl and HBr molecules also bind strongly enough to surface glycerol molecules to enter the liquid after most collisions.

The ultimate fate of HCl and HBr depends on their solubility and reactivity in glycerol. In water, gaseous HBr molecules dissolve more extensively than do HCl molecules ($K_{HBr}(aq) = 7 \times 10^8$ M^2 atm^{-1} vs $K_{HCl}(aq) = 2 \times 10^6$ M^2 atm^{-1} for HX(g) $\rightleftharpoons$ H$^+$(aq) + X$^-$(aq)), mostly because of the greater solvation enthalpy of HBr ($\Delta H^\circ_{HBr}(aq) = -85$ kJ mol^{-1} vs $\Delta H^\circ_{HCl}(aq) = -75$ kJ mol^{-1}). We find below that HCl is less soluble in glycerol ($K_{HCl}(gly) \approx 2 \times 10^3$ M^2 atm^{-1}) than in water and dissolves less exothermically ($\Delta H^\circ_{HCl}(gly) \approx -67$ kJ mol^{-1}). As in water and in ethylene glycol, H$^+$ diffuses much faster than does Cl$^-$ in glycerol,[14,15] suggesting that H$^+$ moves by shuttling along hydrogen-bonded glycerol chains. At high temperatures, HCl and HBr may react directly with glycerol to produce halohydrins such as $XCH_2CH(OH)CH_2OH$,[1] but we could not detect these products in our 294 K experiments.

This paper reports gas uptake measurements as a function of impact energy, approach direction, and gas flux, which are used to determine the fractions of HCl and HBr that enter glycerol and the thermodynamics of HCl dissolution in the bulk liquid. We also use gas−liquid scattering experiments to investigate energy transfer between HCl and HBr and surface glycerol molecules and to monitor DCl → HCl exchange following collisions of DCl. These experiments provide the foundation for studies of near-interfacial HCl dissociation in the following paper.

Experimental Section

Figure 2 depicts the scattering apparatus and an expanded view of the interaction region.[16] Continuously renewed films of glycerol are produced by rotating a 5.0-cm diameter wheel through 75 mL of glycerol in an aluminum reservoir at temperatures T_{gly} of 273−294 K.[17] The glycerol-covered wheel

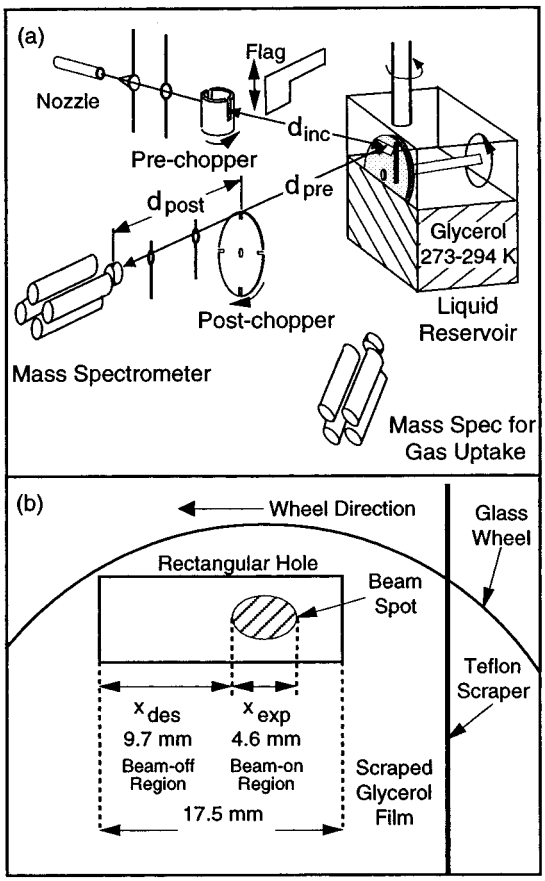

Figure 2. (a) Schematic diagram of the scattering machine. The liquid reservoir is sealed except for a rectangular hole in the front face. (b) Expanded view of the front of the liquid reservoir. The molecular beam enters the rectangular hole from the left at an incident angle of 45°.

is scraped by a cylindrical Teflon bar, leaving behind a vertical film that is 0.18 to 0.26 mm thick at wheel speeds $f = 0.07$ to 0.83 Hz. The incident molecular beam strikes the liquid through a 17.5×6.5-mm^2 rectangular hole in the reservoir, projecting a spot onto the film that is $x_{exp} = 3.2/\cos\theta_{inc}$ mm wide and 3.2 mm high, as shown in panel b. The hole is wider than the maximum x_{exp} value of 6.4 mm to enable the beam to reach the surface at incident angles θ_{inc} from 0 to 60°. The moving liquid is exposed to the incident beam for a time t_{exp} equal to $x_{exp}/(2\pi rf)$, where $r = 1.85$ cm is the distance from the center of the wheel to the center of the beam spot. At $\theta_{inc} = 45°$, t_{exp} ranges from 0.045 to 0.56 s.

Table 1 lists properties of the molecular beams created by expanding mixtures of Ar, HCl, or HBr in H_2, He, and N_2 carrier gases through a 0.07-mm diameter pinhole at 298 K at backing pressures of 800−900 Torr. DCl beams are produced by bubbling the HCl mixtures through a 37 wt % DCl/D_2O solution before expansion through a 403 K nozzle. The HCl isotope contamination was measured to be 6−8% in each DCl beam. The fraction of dimers in the incident beams appears to be small on the basis of observed ion ratios of greater than 25:1 for HX^+/H_2X^+ and $HX^+/(HX)_2^+$ of HCl, HBr, DCl/D_2O, and HCl/H_2O. Measurements of the incident HCl and Ar fluxes were made by comparing beam intensities with a calibrated Ar leak in the scattering chamber. The HCl fluxes in Table 1 are representative and were remeasured for each experiment. We estimate that the absolute fluxes are uncertain to within (+100%, −50%) whereas the relative Ar and relative HCl measurements should be reliable to within ±10%.

TABLE 1: Properties of Incident and Scattered Gases

gas	carrier gas (nozzle temp, K)	$E_{inc} \pm$ fwhm (kJ mol^{-1})	gas flux at surface[a] (cm^{-2} s^{-1})	D^{+b}/M^+ ion ratio	$\langle \Delta E_{IS} \rangle / E_{inc}$
Ar	98% H_2 (298)	95 ± 18	5×10^{15}	<0.01	0.66
	95% He (298)	43 ± 6	5×10^{15}	<0.01	0.59
	pure (298)	6 ± 0.7	1×10^{16}	<0.01	
HCl	98% H_2 (298)	90 ± 15	$\sim 2 \times 10^{15}$	<0.01	0.70
	95% He (298)	40 ± 7	$\sim 4 \times 10^{15}$	<0.02	0.64
	90% N_2 (298)	10 ± 3	$\sim 5 \times 10^{14}$	<0.04	
DCl	~96% H_2 (400)	95 ± 22		<0.02	0.65
	~93% He (400)	53 ± 12		<0.02	0.62
	~88% N_2 (400)	14 ± 5		<0.02	
HBr	98% H_2 (298)	120 ± 24		<0.02	0.81

[a] Incident flux at $\theta_{inc} = 0°$. Values are representative only. [b] Dimer ion/monomer ion ratio in the incident beam, monitored at $(Ar)_2^+/Ar^+$, $(HCl)_2^+/HCl^+$, H_2Cl^+/HCl^+, $(HBr)_2^+/HBr^+$, H_2Br^+/HBr^+, $(DCl)_2^+/DCl^+$, D_2Cl^+/DCl^+, and $(D_2O)(DCl)^+/DCl^+$.

Time-of-flight (TOF) spectra of molecules exiting from the liquid are recorded at $\theta_{inc} = \theta_{fin} = 45°$ by a doubly differentially pumped mass spectrometer. The beam spot is 3.2×4.6 mm^2 at $\theta_{inc} = 45°$, which is close to the dimensions of the umbra region viewed by the spectrometer. As shown in Figure 2a, a "post-chopper" wheel is positioned just after the liquid. The 18.0-cm diameter wheel has four 1.6-mm slots that produce 20-μs gas pulses when the wheel is spun at 150 Hz. The times for molecules to traverse the distance $d_{post} = 19.3 \pm 0.1$ cm between the post-chopper wheel and the mass spectrometer ionizer are recorded by a multichannel scaler in 2-μs bins. All TOF spectra are corrected for triggering offsets and for background evaporation from glycerol molecules dissociatively ionizing at $m/e =$ 36, 38, 39, 40, and 80.

The net uptake of HCl and HBr in glycerol is measured using the reflectivity method.[18,19] The observed uptake $\gamma_{obs}(t_{exp})$ is equal to $(P_{flag} - P_{gly})/(P_{flag} - P_{bkg})$, where P_{flag}, P_{gly}, and P_{bkg} are the HCl or HBr partial pressures when the incident molecules strike a Teflon flag in front of the glycerol, strike the glycerol film, and are blocked from entering the chamber, respectively. $\gamma_{obs}(t_{exp})$ may vary from 0 for no net uptake to 1 for complete uptake. The steady-state partial pressures were measured in 4-minute intervals for HCl and in 30-min intervals for HBr by a second mass spectrometer located in the scattering chamber. The uncertainties in γ_{obs} with changes in t_{exp} and θ_{inc} range from ± 0.003 to ± 0.01. The month-to-month variations in γ_{obs} may be as large as ± 0.04 because of changes in incident HCl flux and adsorption of HCl and HBr on the chamber walls.

Ar, HBr, HCl, and DCl Uptake

Analysis Procedure. We measure the net uptake γ_{obs} of HCl and HBr in glycerol as a function of gas exposure time t_{exp} to extract the initial uptake $\beta(E_{inc},\theta_{inc})$ and the characteristic residence time τ of HCl and HBr in solution. Figure 2b shows that a patch of glycerol on the rotating wheel passes through two regions as it moves in front of the rectangular hole in the reservoir. In the "beam-on" region of width x_{exp}, the patch is exposed to the incident HX beam for a time t_{exp}. In this region, a fraction $\beta(E_{inc},\theta_{inc})$ of the impinging molecules dissolves in glycerol either as HX or as H^+ and X^- after first dissociating in the interfacial region (β is equal to or larger than the mass accommodation coefficient α because it potentially includes this second $H^+ + X^-$ entry channel[20]). As shown below, all HX molecules that enter glycerol eventually dissociate and exist as H^+ and Cl^- in solution. A fraction of the dissolved H^+ and X^- then recombine and desorb within time t_{exp} in the beam-on region. This desorption reduces the net uptake. The film then passes into the beam-off region of width x_{des}, where a fraction of the remaining H^+ and X^- recombine and desorb for an additional time t_{des} without being replenished by the impinging beam. The observed net uptake $\gamma_{obs}(t_{exp}, t_{des}; E_{inc},\theta_{inc})$ can be expressed as integrals over the instantaneous uptake and desorption in the two regions:

$$\gamma_{obs} = \frac{\int_0^{t_{exp}} \gamma_{exp}(t)\, F_{beam}\, dt - \int_{t_{exp}}^{t_{exp}+t_{des}} \gamma_{des}(t)\, F_{beam}\, dt}{F_{beam} t_{exp}} \quad (1)$$

The first integral accounts for gas uptake in the beam-on region, where F_{beam} is the incident gas flux and $\gamma_{exp}(t)\, F_{beam} = F_{in} - F_{des}(t)$ is the difference between the flux of molecules entering the liquid, $F_{in} = \beta(E_{inc}, \theta_{inc})\, F_{beam}$, and the time-dependent flux of molecules desorbing from the liquid, $F_{des}(t)$.[20,21] As described in the Appendix, $\gamma_{exp}(t) = \beta(E_{inc},\theta_{inc})\, [1 - c(x = 0, t)^2/c^{*2}]$ is the instantaneous uptake coefficient in the beam-on region, where $c(x, t)$ is the solution concentration of X^- and H^+ at depth x and time t and c^* is the saturation value for the chosen HX impinging flux. The dependence of γ_{exp} on c^2 arises from the second-order recombination of X^- and H^+ into HX. Figure A.1 in the Appendix shows that $\gamma_{exp}(t)$ drops from the maximum value of $\beta(E_{inc}, \theta_{inc})$ at $t = 0$, when there are no dissolved molecules to evaporate, to a lower value at later times as dissolved molecules begin to desorb. The second integral in eq 1 accounts for gas desorption in the beam-off region, given by $\gamma_{des}(t)F_{beam} = F_{des}(t)$, where the desorption coefficient $\gamma_{des}(t) = \beta(E_{inc}, \theta_{inc})\, [c(x = 0, t)^2/c^{*2}]$ drops from its maximum value at $t = t_{exp}$ to a value of 0 as $t \rightarrow \infty$ and the liquid is fully depleted of gas. The geometry in Figure 2b determines the duration t_{des} of the beam-off region, yielding $t_{des} = (4.4 \cos \theta_{inc} - 1)t_{exp}$, which is equal to $2.1t_{exp}$ at $\theta_{inc} = 45°$. A numerical procedure for calculating $\gamma_{exp}(t)$ and $\gamma_{des}(t)$ is described in the Appendix.

The time dependence of $\gamma_{exp}(t)$ and $\gamma_{des}(t)$ is parametrized by τ, the characteristic residence or solvation time of HCl dissolved in glycerol: τ is the time for $\gamma_{exp}(t)$ to drop from its initial value of $\beta(E_{inc}, \theta_{inc})$ to $0.48\beta(E_{inc}, \theta_{inc})$ as more HCl enters solution and the flux of desorbing HCl increases.[16,20−22] This residence time can be expressed as

$$\tau = D_{HCl}\left(\frac{4H^* R T_{gly}}{\beta_{th} v_{th}}\right)^2 \quad (2)$$

D_{HCl} and H^* are the joint diffusion coefficient and solubility of H^+ and Cl^- in glycerol, and β_{th} is the fraction of HCl molecules in an impinging thermal gas (with average velocity v_{th}) that enter glycerol as either HCl or after dissociating into H^+ and Cl^- in the interfacial region. As noted in the Appendix, eq 2 is valid when a liquid is exposed to ambient gas or to a nonthermal beam.

The values of $\beta(E_{inc}, \theta_{inc})$ and τ are extracted from the observed uptake by using eq 1 to fit a graph of $\gamma_{obs}(t_{exp})$ versus

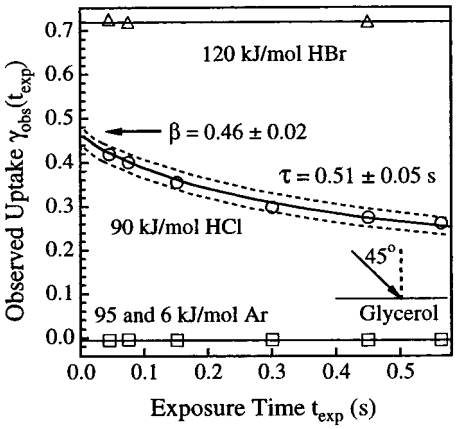

Figure 3. Observed gas uptake versus exposure time for HCl, HBr, and Ar striking glycerol at 294 K at $\theta_{inc} = 45°$. Only γ_{obs}(HCl) depends on exposure time t_{exp}. The solid and dashed lines are fits to the HCl data using eq 1 and the indicated values of the initial uptake β and residence time τ. The flux of HCl molecules entering the liquid is approximately 3×10^{14} cm^{-2} s^{-1}.

t_{exp}. The ways in which $\beta(E_{inc}, \theta_{inc})$ and τ vary with incident angle θ_{inc}, incident energy E_{inc}, glycerol temperature T_{gly}, and HX incident flux F_{beam} are investigated below.

Gas Uptake Versus Exposure Time. Figure 3 is a plot of γ_{obs} versus t_{exp} for Ar, HCl, and HBr colliding with 294 K glycerol at $\theta_{inc} = 45°$. γ_{obs}(Ar) is measured to be -0.005 ± 0.004 for $E_{inc} = 6$ and 95 kJ mol^{-1} over $t_{exp} = 0.038-0.48$ s. This zero uptake indicates that any argon atoms that dissolve in glycerol desorb within the shortest exposure time of 0.045 s. The slightly negative value of -0.005 is due to differences in pumping speeds in the scattering chamber when the Teflon flag is in the open and blocking positions.

The net uptake for HBr at $E_{inc} = 120$ kJ mol^{-1} is 0.72 ± 0.04, independent of exposure time to within ± 0.01 within a given run.[23] This measurement demonstrates that 7 of 10 impinging HBr molecules dissolve in glycerol even at collision energies that are 25 times the thermal energy of $2RT_{gly} = 5$ kJ mol^{-1}. The high value of 0.72 is not due to ballistic penetration of HBr into glycerol, a process that would cause the uptake to increase at higher impact energy.[24] Studies of HCl below and of HBr and HCl in sulfuric acid show instead that gas entry is less likely at higher E_{inc}. These experiments imply that uptake is limited by the fraction of molecules that dissipate their excess energy and thermally equilibrate at the surface.[16] Fits to the ± 0.01 uncertainty in γ_{obs}(HBr) over the 0.4 s interval in Figure 3 yield HBr residence times that exceed 10 s. In this case of longtime solvation, the initial uptake equals γ_{obs}, and $\beta_{HBr}(E_{inc} = 120$ kJ mol^{-1}, $\theta_{inc} = 45°)$ is 0.72.

Figure 3 also shows that the net uptake of HCl decreases from 0.42 to 0.28 at $E_{inc} = 90$ kJ mol^{-1} as the exposure time is increased from 0.045 to 0.56 s. This large drop in γ_{obs} implies that the solvation time for HCl must be on the order of t_{exp} and therefore shorter than the residence time for HBr, a stronger acid. The extracted residence time and initial uptake are $\tau = 0.51 \pm 0.05$ s and $\beta_{HCl}(90$ kJ mol^{-1}, $45°) = 0.46 \pm 0.02$. The dashed lines in Figure 3 are fits corresponding to the specified uncertainties in β and τ. These values indicate that 46% of the HCl molecules that strike the glycerol surface at $E_{inc} = 90$ kJ mol^{-1} and $\theta_{inc} = 45°$ enter the liquid and remain on average for one-half second before desorbing. Additional examples of time-dependent HCl uptake are shown in Figures 9 and 11 for 10 and 90 kJ mol^{-1} HCl.

TOF Spectra of Ar, HBr, and HCl. To identify the pathways that are responsible for gas uptake, we recorded TOF spectra of Ar, HBr, and HCl scattering from glycerol at $t_{exp} = 0.045$ and 0.45 s. The spectra in Figure 4 are plots of the mass spectrometer signal $N(t)$ versus arrival time t at $\theta_{inc} = \theta_{fin} = 45°$. $N(t)$ is proportional to the number density and is used to calculate the relative flux or probability, $P(E_{fin})$, that a molecule will leave the liquid with translational energy E_{fin} at angle θ_{fin}. The translational energy distributions in Figure 5 at $t_{exp} = 0.45$ s are computed from the relations $P(E_{fin}) \propto N(t)\, t^2$ and $E_{fin} = (1/2)(m_{gas})(d_{post}/t)^2$.

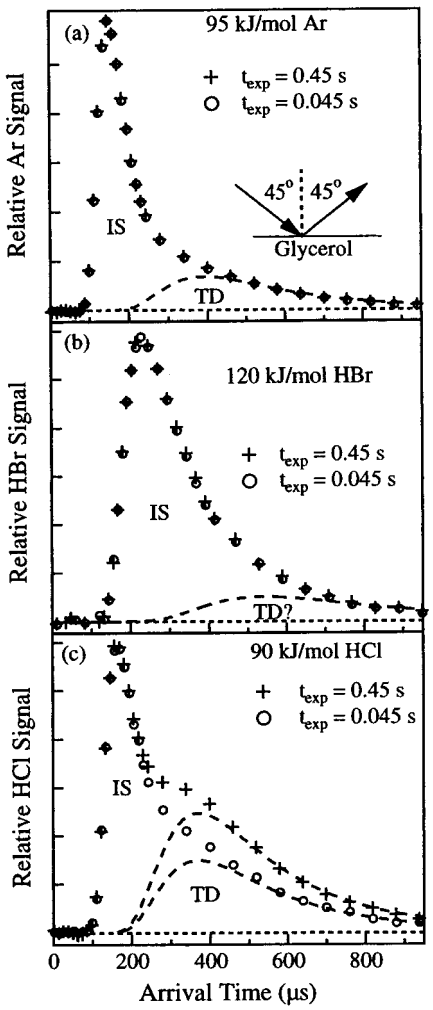

Figure 4. Time-of-flight (TOF) spectra of Ar, HBr, and HCl impinging on glycerol for exposure times t_{exp} of 0.45 and 0.045 s. IS and TD refer to direct inelastic scattering and thermal desorption. The dashed lines are Maxwell−Boltzmann fits to the TD components at $T_{gly} = 294$ K.

The Ar and HCl energy distributions in panels a and c of Figure 5 are bimodal, corresponding to direct inelastic scattering (IS) at short arrival times (high final energies) and thermal desorption (TD) at long arrival times (low final energies).[6,25] The TD components are fit to a Boltzmann distribution, $P_{TD}(E_{fin}) = E_{fin}(RT_{gly})^{-2} \exp[-E_{fin}/RT_{gly}]$, at $T_{gly} = 294$ K. The IS component is assigned to the difference between $P(E_{fin})$ and $P_{TD}(E_{fin})$ such that $P_{IS}(E_{fin}) = 0$ at $RT_{gly} = 2.4$ kJ mol^{-1}. Table 1 lists the average fractional energy transfers, $\langle \Delta E_{IS} \rangle / E_{inc}$, for inelastic scattering at $\theta_{inc} = \theta_{fin} = 45°$. On average, 95 kJ mol^{-1} Ar and 90 kJ mol^{-1} HCl transfer 66 and 70% of their incident energy, respectively, to interfacial glycerol molecules during an inelastic collision, while 120 kJ mol^{-1} HBr molecules (Figures 4b and 5b) transfer 81% of their incident energy. These energy losses reflect the significant transfer of momentum that occurs when an impinging Ar, HCl, or HBr strikes the relatively

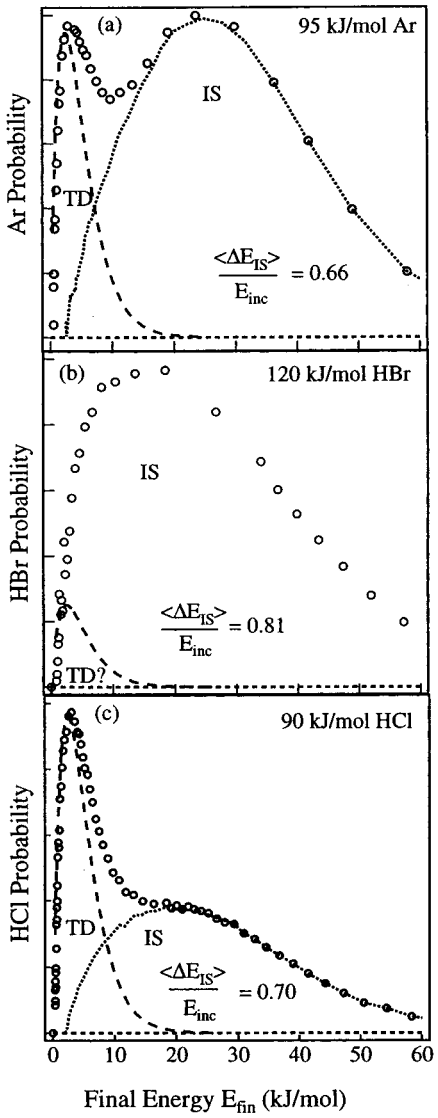

Figure 5. Energy distributions $P(E_{fin})$ for Ar, HBr, and HCl obtained by direct inversion of the TOF spectra in Figure 4 for $t_{exp} = 0.45$ s. The dashed lines are Boltzmann distributions at $T_{gly} = 294$ K. $\langle \Delta E_{IS} \rangle / E_{inc}$ is the average fractional energy transfer in the IS channel.

light glycerol molecule ($m_{Ar}/m_{glycerol} \approx m_{HCl}/m_{glycerol} = 0.4$ and $m_{HBr}/m_{glycerol} = 0.9$).[26] The inelastic energy transfer for HCl is only slightly larger than for Ar, the inert gas atom closest in mass, implying that there is little HCl internal excitation during a direct inelastic collision. Similar values for Ar and HCl inelastic energy transfer have been observed previously in collisions with sulfuric acid and water ice.[16,27,28]

Intensity changes in TOF spectra recorded at different exposure times reveal whether solute molecules desorb on the 10^{-2} to 10^{0} s experimental time scales of t_{exp}.[29] The IS components within each panel in Figure 4 are identical in intensity and shape at $t_{exp} = 0.045$ and 0.45 s, as expected for the picosecond duration of a direct inelastic collision. The distinct TD component for argon in Figure 5a indicates that some Ar atoms thermally equilibrate at the surface and then desorb, but their net zero uptake and identical intensities at $t_{exp} = 0.045$ and 0.45 s both indicate that the Ar residence times are much shorter than 0.045 s.[30]

The $P(E_{fin})$ distribution for HBr in Figure 5b does not show evidence of a distinct thermal desorption component. The TD fit in panel b is limited to 5% of the overall distribution and is likely due to HBr molecules that lose most of their energy upon impact and scatter at low final velocities. The absence of a distinct TD component implies that nearly all HBr molecules that thermally equilibrate upon collision with glycerol enter the liquid and do not desorb for long times. The identical TOF spectra at $t_{exp} = 0.045$ and 0.45 s confirm that HBr must dissolve for times much longer than t_{exp}. This longtime solvation is responsible for the constant γ_{obs}(HBr) value of 0.72 in Figure 3. Assuming that no HBr molecules undergo trapping and desorption, the remaining 28% of the impinging 120 kJ mol^{-1} HBr molecules that escape solvation are restricted to those that scatter inelastically from the surface. The nearly complete disappearance of thermalized HBr molecules and their longtime solvation suggest that HBr readily protonates glycerol in the near-interfacial region and remains dissociated in the bulk liquid because of the stability of solvated Br^- and H^+.

In contrast to the Ar and HBr distributions, the HCl TOF spectra in Figure 4c vary with exposure time. This time dependence is due to an increase in thermal desorption at longer t_{exp}, as shown by the Maxwell−Boltzmann distributions fits at $t_{exp} = 0.045$ and 0.45 s. The TD signal grows with increasing t_{exp} as HCl molecules that have entered the liquid are given more time to evaporate. The higher HCl desorption flux in turn causes decreasing HCl uptake with t_{exp} in Figure 3. These TOF spectra confirm that a large fraction of the TD signal can be associated with HCl solvation on the 10^{-1} s time scale, as denoted by p_{solv} in Figure 1. This time dependence is used later to extract ΔG°_{HCl}(gly) and ΔH°_{HCl}(gly) for HCl dissolution in glycerol.

D → H Exchange in DCl Collisions. The fate of HCl molecules that enter glycerol was investigated by substituting DCl for HCl at $E_{inc} = 53$ kJ mol^{-1} and searching for the production of D → H-exchanged HCl. The TOF spectra at $m/e = 38$ ($H^{37}Cl$) in Figure 6a show that D → H exchange occurs and that the exiting HCl molecules have two characteristics: they desorb in a Maxwell−Boltzmann distribution at $T_{liq} = 294$ K (dashed lines), as confirmed by the energy distribution in panel c, and they desorb more strongly at longer t_{exp}, just as in Figure 4c. These results demonstrate that DCl → HCl exchange accompanies the 10^{-1} s solvation of DCl in glycerol. The Appendix shows that the ratio of the thermal desorption intensities of 0.42 ± 0.03 at the two exposure times yields a residence time for HCl of $\tau = 0.17 \pm 0.05$ s. As described below, this residence time differs from the 0.51 s value in Figure 3 because of the different HCl and DCl fluxes in the two impinging beams.

Trapping and Desorption in DCl Collisions. Figure 6b shows that TOF spectra recorded at $m/e = 39$ ($D^{37}Cl$) are identical at $t_{exp} = 0.045$ and 0.45 s, indicating that DCl molecules that do not undergo D → H exchange do not enter the liquid for long times. We show in the following paper that this time is less than 10^{-6} s. However, the corresponding DCl translational energy distribution in panel d peaks at low energies, suggesting that it is composed not only of DCl molecules that scatter inelastically from the surface but also of DCl molecules that thermalize and desorb before undergoing D → H exchange. This trapping−desorption component is modeled by a 294 K Boltzmann distribution, denoted as a dashed line in panel d.

Figure 7 provides evidence that this low-energy component is due mostly to thermal desorption of DCl and not to inelastic scattering at near-thermal energies. The DCl collision energy was increased to 95 kJ mol^{-1}, and the glycerol temperature was lowered to 273 K to separate the IS and TD components more widely in arrival time. The HCl spectrum in panel a shows that

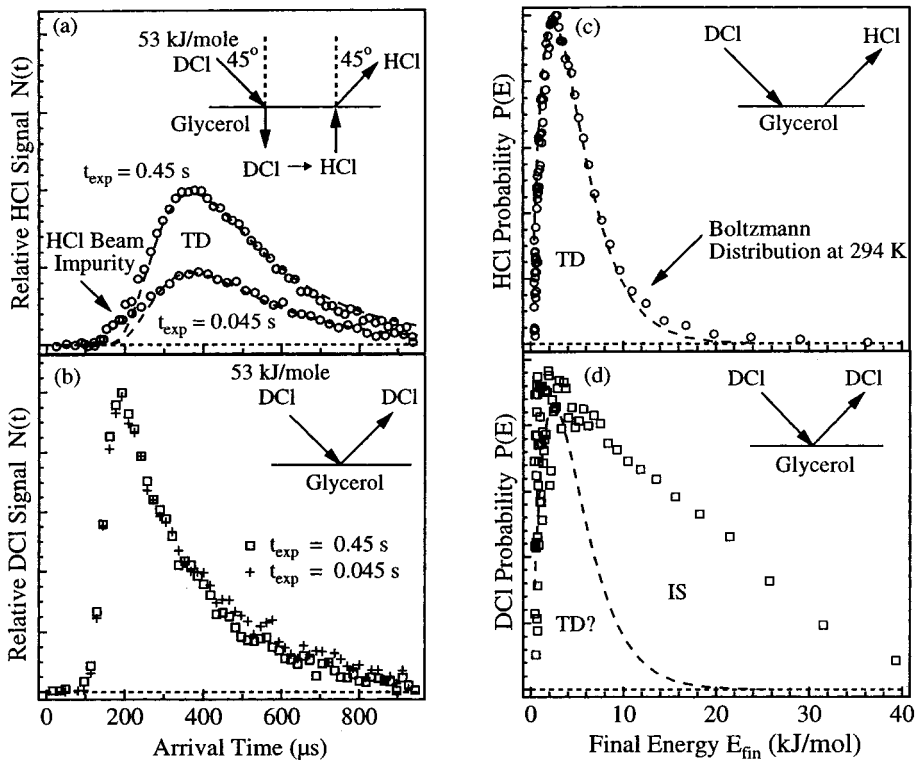

Figure 6. (a) TOF spectra of D → H-exchanged $H^{37}Cl$ ($m/e = 38$) following collisions of 53 kJ/mol DCl with glycerol at $t_{exp} = 0.045$ and 0.45 s. The weak signal at short arrival times is due to inelastic scattering of a 6% HCl impurity in the DCl beam. The dashed lines are Maxwell−Boltzmann distributions at $T_{gly} = 294$ K. (b) TOF spectra of unexchanged $D^{37}Cl$ ($m/e = 39$) at $t_{exp} = 0.045$ and 0.45 s plotted relative to the signal in panel a. (c) Translational energy distribution for the HCl TOF spectrum at $t_{exp} = 0.45$ s in panel a. (d) Translational energy distribution for the DCl TOF spectrum in panel b at $t_{exp} = 0.45$ s. The dashed lines in panels c and d are best-fit Boltzmann distributions at $T_{gly} = 294$ K.

there is still substantial D → H-exchanged HCl thermally desorbing from glycerol. The HCl signal from D → H exchange is weaker than at $E_{inc} = 53$ kJ mol^{-1} because higher impact energies reduce the fraction of molecules that can dissipate their energy and thermalize upon collision. At this higher impact energy and lower temperature, the DCl energy distribution in panel b is distinctly bimodal, implying that two separate processes are taking place. Most of the low-energy component is fit by a Boltzmann distribution at 273 K, and the higher-velocity DCl molecules are attributed to direct inelastic scattering. The existence of the low-energy peak confirms that some DCl molecules survive collisions with glycerol by dissipating their excess energy but desorbing before exchange can occur. In the next paper, we show that this peak corresponds to the immediate desorption of one in five thermalized DCl molecules.

Incident Angle and Energy Dependence of HCl and HBr Initial Uptake and Trapping. We return in this section to uptake measurements to investigate how the overall probabilities of HCl and HBr entry into bulk glycerol depend on impact energy and approach direction. Measurements at exposure times from 0.045 to 0.45 s were made for 10, 40, and 90 kJ mol^{-1} HCl, 120 kJ mol^{-1} HBr, and 53 and 95 kJ mol^{-1} DCl at $\theta_{inc} = 0-60°$. The initial uptake values $\beta(E_{inc}, \theta_{inc})$ extracted from these data are plotted in Figure 8. The upper panel shows that the initial uptake values for high incident energy HCl and HBr decrease at more glancing incidence (higher θ_{inc}), dropping from 0.84 to 0.68 for 120 kJ mol^{-1} HBr and from 0.56 to 0.48 for 90 kJ mol^{-1} HCl over an angular range of 60°. In contrast, the β values for lower-energy HCl vary more modestly with θ_{inc} and reach a nearly constant value of 0.67 at $E_{inc} = 10$ kJ mol^{-1} ($4RT_{gly}$). The lower panel emphasizes that the initial uptake decreases steadily with increasing collision energy at a fixed incident angle. These trends have also been observed for collisions of ethanol, dimethyl ether, and formic acid with 99 wt % sulfuric acid.[19]

The initial uptake values in Figure 8 are less than 1 because some impinging HCl and HBr molecules scatter directly from the surface and because 20% of the thermalized HCl molecules desorb before entering the bulk liquid. In the next paper, we show that the remaining 80% of thermalized HCl molecules are partitioned into 73% bulk solvation and 7% immediate exchange and desorption and that these fractions do not vary with HCl incident energy. The invariance of these fractions with E_{inc} implies that HCl molecules impinging on glycerol first dissipate their excess energy and become momentarily trapped, followed by reaction and desorption processes that are independent of the initial trajectories. The solvation probability can then be expressed as a product of the trapping probability and the fraction that dissolves: $\beta(E_{inc}, \theta_{inc}) = p_{trap}(E_{inc}, \theta_{inc})f_{solv}$ where f_{solv} is independent of E_{inc} and θ_{inc}.[16] p_{trap} can be obtained from this expression by using the β values in Figure 8 and the fractions $f_{solv}(HCl) = 0.73$ and $f_{solv}(HBr) \approx 1$ (which is based on the absence of HBr thermal desorption in Figure 3). The p_{trap} values for HCl are given by the right-hand axes in Figure 8, and $p_{trap} \approx \beta_{HBr}(E_{inc}, \theta_{inc})$ for HBr. The trapping probabilities follow the same trend as do the initial uptake values and decrease steadily with a more glancing approach angle and higher impact energies.

The trends in Figure 8 are in accord with kinematic models of hard sphere-like collisions. At $E_{inc} \gg RT$, these models predict that gas−surface energy transfer decreases at more glancing angles (larger θ_{inc}) as the impact parameter becomes larger and less momentum is directed along the line-of-centers between the HX and surface glycerol molecules.[26,31] In the absence of ballistic penetration, the thermalization rates will also decrease with increasing E_{inc} because more kinetic energy must be

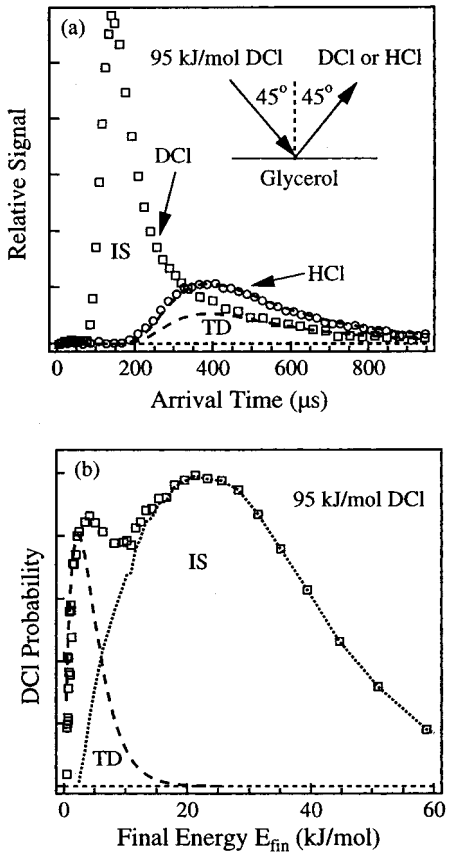

Figure 7. (a) TOF spectra of DCl and HCl following collisions of 95 kJ/mol DCl with glycerol at $t_{exp} = 0.45$ s and at $T_{gly} = 273$ K. (b) DCl energy distribution for the TOF spectrum in panel a, providing evidence for a distinct trapping−desorption component. The dashed line is a Boltzmann distribution at $T_{gly} = 273$ K.

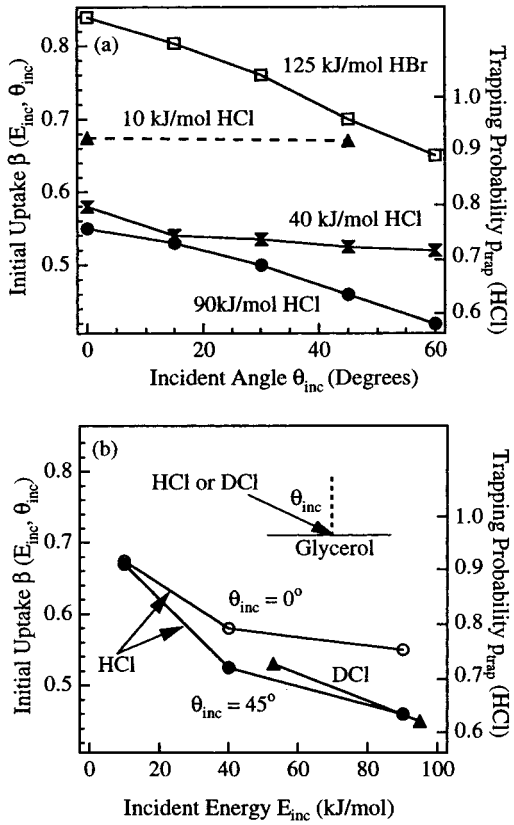

Figure 8. (a) Initial uptake versus incident angle for HCl and HBr. (b) Initial uptake versus incident energy for HCl and DCl at $\theta_{inc} = 45°$ (●, ▲) and $\theta_{inc} = 0°$ (○). Values of β for HCl were obtained by fitting $\gamma_{obs}(t_{exp})$ versus t_{exp}. The right-hand axis is the estimated trapping probability for HCl given by $p_{trap} = \beta_{HCl}/0.73$. Values of $\beta = p_{trap}$ for HBr are equal to γ_{obs}.

dissipated during the gas−surface encounter. At the lowest energy of 10 kJ mol^{-1}, the trapping probability is greater than 0.9, implying that p_{trap} should be close to 1 for HCl molecules striking glycerol in a thermal gas at $\langle E_{inc} \rangle = 2RT_{liq} = 5$ kJ mol^{-1}. Trapping probabilities near 1 have been measured previously for thermal-energy collisions of HCl with water ice,[28,32,33] where the gas−surface binding energy of ∼30 kJ mol^{-1} provides a deep well for capturing the incoming HCl molecule.[33−35] Similarly strong hydrogen bonding may also be responsible for binding HCl to the surface OH groups of glycerol long enough for 80% of the thermalized HCl molecules to dissociate in the interfacial or deeper regions of the liquid. Although sum frequency experiments indicate that the surface of glycerol contains few dangling OH groups,[11] the 1:1 H/O ratio implies that there must be a significant number of O atom lone pairs at the surface that can momentarily bind to the H atoms of thermalized HCl molecules.

Last, we note that the initial uptake of a thermal gas of HCl in water at 294 K is measured to be 6−10%,[36,37] much less than the 68% uptake of HCl in glycerol at $E_{inc} = 10$ kJ mol^{-1}. The uptake of HBr in water at 281−283 K is 7−14%,[36,37] again less than the 70% uptake in glycerol even at $E_{inc} = 120$ kJ mol^{-1}. These measurements point to potentially significant differences in the initial interactions of HCl and HBr with water and glycerol, as discussed in the next paper.

Flux Dependence of HCl Uptake. Figure 9 illustrates how the net uptake of HCl depends on the flux of the impinging beam. The upper panel displays $\gamma_{obs}(t_{exp})$ for 10 kJ mol^{-1} HCl striking glycerol at $\theta_{inc} = 0°$. As the HCl flux is halved from 5.0 to 2.5 × 10^{14} molecules cm^{-2} s^{-1} by pulling the molecular beam nozzle further from the surface, the initial uptake values remain equal (0.66 and 0.67), but the HCl residence time nearly doubles from 0.60 to 1.0 s.

The incident HCl flux can also be lowered by increasing the angle of impact. The lower panel in Figure 9 is a plot of γ_{obs} versus t_{exp} for 90 kJ mol^{-1} HCl at $\theta_{inc} = 15°$, 45°, and 60°. The initial uptake decreases from 0.53 to 0.45, and the residence time τ increases from 0.30 to 0.90 s as the HCl molecules approach the surface at more glancing incidence. The flux of HCl entering glycerol decreases at higher θ_{inc} for two reasons: the incident beam is projected over a greater area on the surface at larger θ_{inc} because $F_{beam}(\theta_{inc}) = F_{beam}(0°) \cos \theta_{inc}$, and as shown in Figure 8a, β decreases with increasing θ_{inc} because of the more glancing nature of the impact. These factors lead to reactive fluxes $F_{in} = \beta(E_{inc}, \theta_{inc})\, F_{beam}(\theta_{inc})$ of 1.4 × 10^{15}, 6.0 × 10^{14}, and 3.0 × 10^{14} cm^{-2} s^{-1} at $\theta_{inc} = 15°$, 45°, and 60°, respectively.

The increase in residence time with decreasing reactive flux in Figure 9 is analogous to bulk-phase, second-order reactions in which the half-life varies inversely with the initial reagent concentration. If the H$^+$ ions generated by dissolved HCl are much more numerous than H$^+$ from autoionization of glycerol, then the HCl flux will control the H$^+$ concentration and therefore the rate of H$^+$ and Cl$^-$ recombination and their residence times in solution. As described below, this dependence predicts an inverse relation between the residence time τ and the reactive flux F_{in}. We attempted to test this prediction by varying F_{in} from 0.1 × 10^{15} to 3 × 10^{15} cm^{-2} s^{-1} (∼0.1 to 3 HCl monolayers per second).[38] The data in Figure 10 show that τ increases with $1/F_{in}$, but the measurements are too noisy to

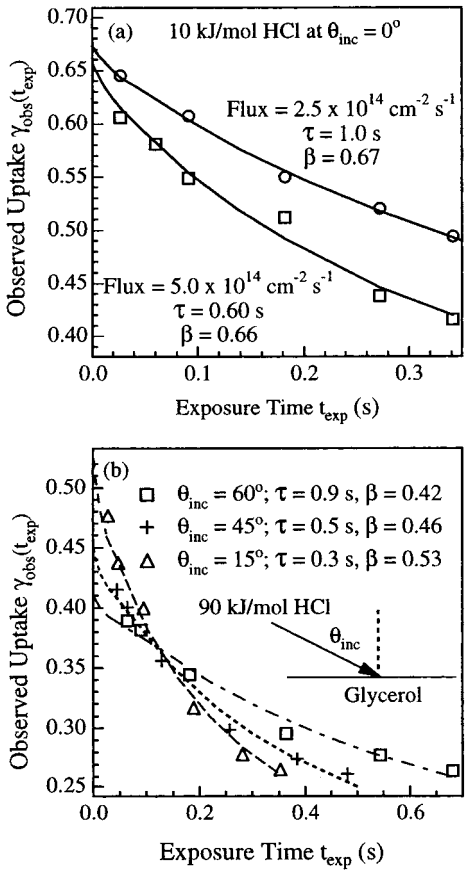

Figure 9. (a) Gas uptake versus exposure time for 10 kJ/mol HCl at two incident gas fluxes, showing that τ depends on flux. (b) Gas uptake versus exposure time for 90 kJ/mol HCl at different incident angles, showing that τ also depends on θ_{inc}.

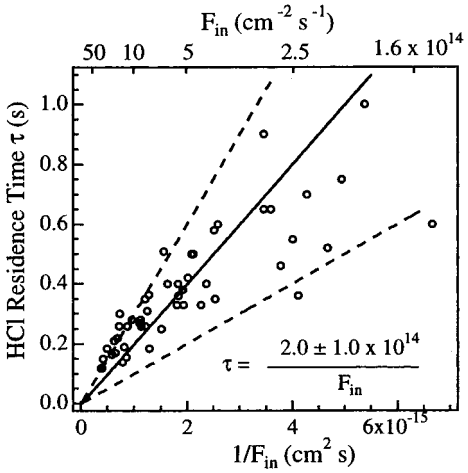

Figure 10. HCl residence time versus the inverse of the flux of molecules entering the liquid, $F_{in} = \beta(E_{inc}, \theta_{inc})\, F_{beam}$. The solid and dashed lines are plots of $\tau(s) = 2.0 \pm 1.0 \times 10^{14}/F_{in}$ (cm^{-2} s^{-1}).

determine the functional dependence precisely. The best fits to an inverse relation lie within the range of $\tau = (2.0 \pm 1.0) \times 10^{14}/F_{in}$, with τ in seconds and F_{in} in molecules cm^{-2} s^{-1}.

The measured HCl residence times of 0.1 to 1 s are much longer than the predicted diffusion-limited recombination times of H^+ and Cl^-. The recombination rate can be estimated from $k_{diff}[H^+] = 4\pi(D_{H^+} + D_{Cl^-})R_{ion}[H^+] \approx 5 \times 10^5$ s^{-1} using summed diffusion coefficients[39] ($D_{H^+} + D_{Cl^-}$) $\approx 5 \times 10^{-7}$ cm^{-2} s^{-1}, the effective ion contact distance $R_{ion} \approx 10$ Å,[40] and $[H^+] = 10^{-3}$ M. This high rate implies that H^+ and Cl^- come into

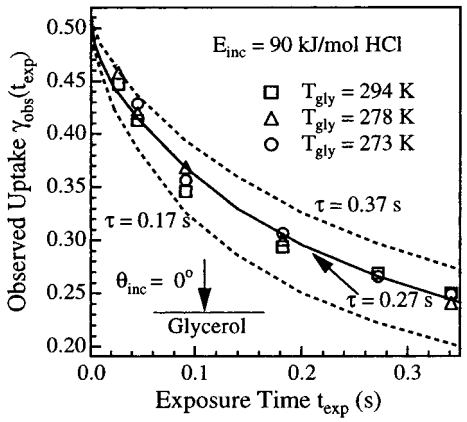

Figure 11. Observed HCl uptake versus exposure time at $T_{gly} = 273$, 278, and 294 K. The best-fit values are $\tau = 0.29$ s and $\beta = 0.50$ for 294 K, $\tau = 0.25$ s and $\beta = 0.51$ for 278 K, and $\tau = 0.27$ s and $\beta = 0.51$ for 273 K. The solid and dashed lines are fits to $\tau = 0.27 \pm 0.10$ s.

contact 10^5 or more times in glycerol during a 1 s residence time before they recombine a final time in the near-interfacial region and are propelled by thermal motions from the surface as molecular HCl. As shown in Figures 5−7, the desorption signals are well fit by Maxwell−Boltzmann distributions at 294 and 273 K, indicating that the reformed HCl molecules thermally equilibrate before they desorb from the surface.

Temperature Dependence of HCl Uptake. Figure 11 displays the variations in γ_{obs} with t_{exp} at $T_{gly} = 273$, 278, and 294 K for 90 kJ mol^{-1} HCl striking glycerol at $\theta_{inc} = 0°$. The viscosity changes from 12 000 to 1300 cP over this temperature range, but the measurements indicate that γ_{obs} varies only weakly over the 21 K interval. The three data sets are fit with residence times between 0.25 and 0.29 s and with initial uptake values between 0.50 and 0.51. The relation between τ and F_{in} and the weak dependence of γ_{obs} on T_{gly} are used below to estimate the free energy, enthalpy, and entropy of HCl dissolution in glycerol.

HCl Residence Times and Solution Thermodynamics

HCl molecules dissolve in glycerol for times that depend on their solubility and mobility according to eq 2. An analysis of these times yields ΔG°_{HCl}(gly) and ΔH°_{HCl}(gly) for bulk-phase dissolution of HCl in glycerol. Figure 10 shows that the residence times vary approximately inversely with the incident HCl flux, ranging from 1 to 0.1 s at fluxes of 0.2×10^{15} to 2×10^{15} cm^{-2} s^{-1}. This inverse relation can be derived by applying eq 2 to molecules that dissociate in solution. The equilibrium constant for $HCl(g) \rightleftharpoons H^+(gly) + Cl^-(gly)$ is first written as $K_{HCl}(gly) = [H^+][Cl^-]/P_{HCl}$. The native $[H^+]$ from glycerol ionization is assumed to be less than 10^{-6} M on the basis of its weak dissociation constant in water of 7×10^{-15} and the fact that the dielectric constant of glycerol is lower than that of water. The H^+ concentration due to impinging HCl can be estimated by dividing the net number of HCl molecules that dissolve by the approximate diffusion depth, $(Dt_{exp})^{1/2}$. This depth is 1×10^{-4} cm for a diffusion coefficient D_{HCl} of 4×10^{-8} cm^2 s^{-1} (see below) and an exposure time t_{exp} of 0.2 s. The average H^+ concentration, $\langle F_{net}\rangle t_{exp}/(Dt_{exp})^{1/2}$, is 2×10^{-3} M for typical values of $\langle F_{net}\rangle = \langle \gamma_{obs}(t_{exp})\rangle F_{beam} \approx 5 \times 10^{14}$ cm^{-2} s^{-1}. The fluxes and exposure times used for constructing Figure 10 generate near-surface concentrations of approximately 3×10^{-4} to 1×10^{-2} M. The H^+ ions in solution therefore arise almost entirely from impinging HCl rather than from the

autoionization of glycerol, indicating that $[H^+]$ and $[Cl^-]$ are nearly equal and that $K_{HCl}(gly) \approx [Cl^-]^2/P_{HCl}$.

The Henry's law solubility of HCl in glycerol, H^* (M atm^{-1}), that appears in eq 2 is given by $([HCl] + [Cl^-])/P_{HCl} \approx [Cl^-]/P_{HCl} = (K_{HCl}/P_{HCl})^{1/2}$, assuming that all dissolved HCl molecules are dissociated. The HCl gas pressure can be expressed in terms of the reactive flux, $F_{in} = \beta(E_{inc}, \theta_{inc})\, F_{beam}$, by expressing F_{in} using an effective gas concentration, P_{HCl}/RT_{gly}, through the relation F_{in} (cm^{-2} s^{-1}) $= \beta_{th}(P_{HCl}/RT_{gly})(\upsilon_{th}/4)(1000/N_A)$. In this equation, $R = 0.08206$ atm M^{-1} K^{-1} and N_A is Avogadro's constant. Substituting these expressions into eq 2 yields

$$\tau = \left(\frac{4D_{HCl}K_{HCl}RT_{gly}}{\beta_{th}\upsilon_{th}F_{in}}\right)\left(\frac{1000}{N_A}\right) \qquad (3)$$

This equation predicts that the residence time should vary inversely with the reactive flux, as found approximately in Figure 10. Deviations from this inverse relation may be due to systematic errors in measurements of the incident HCl flux and to the neglect of ion activity coefficients (as described in ref 41).

Equation 3 can be used to determine $K_{HCl}(gly)$ and $\Delta G^\circ_{HCl}(gly)$ for HCl in glycerol if the values of β_{th} and D_{HCl} are known. Figure 8 indicates that β_{th} is approximately 0.7 at thermal collision energies. The joint diffusion coefficient for H^+ and Cl^-, $D_{HCl} = D_{H^+}\, D_{Cl^-}/(D_{H^+} + D_{Cl^-})$, can be estimated from conductance measurements and the relation $D_{HCl} = (RT_{gly}/F^2)(T_{H^+}\, \lambda^\infty_{Cl^-})$, where T_{H^+} and $\lambda^\infty_{Cl^-}$ are the transference number for H^+ and the equivalent conductance for Cl^- at infinite dilution, respectively, and F is Faraday's constant. The value of $\lambda^\infty_{Cl^-}$ in pure glycerol at 298 K is 1.8×10^{-5} m^2 ohm^{-1} mol^{-1}, and T_{H^+} is 0.93 for 0.025 M HCl in 98.48 mol % glycerol/1.62 mol % water.[14,15] These values yield $D_{HCl} \approx D_{Cl^-} = 4 \times 10^{-8}$ cm^2 s^{-1} at 294 K, approximately 400 times smaller than the diffusion coefficient of HCl in water. Using eq 3 and the product τF_{in} of 2.0×10^{14} cm^{-2} from Figure 10, we find that $K_{HCl}(gly) = 2300^{+3000}_{-1500}$ M^2 atm^{-1} and $\Delta G^\circ_{HCl}(gly) = -19 \pm 2$ kJ mol^{-1} at 294 K. The error bars include the experimental uncertainties in F_{in} and in the slope τF_{in} in Figure 10. $K_{HCl}(gly)$ is slightly larger than the dissociation constant for HCl in ethylene glycol of 1300 M^2 atm^{-1},[42] but it is 1400 times smaller than the value in water, resulting in a free energy that is 18 kJ mol^{-1} less favorable.[43] For the same HCl gas pressure, the Henry's law solubilities and the H^+ and Cl^- concentrations are approximately 40 times greater in water than in glycerol.

The enthalpy of solvation of HCl in glycerol can also be estimated by noting that τ is approximately constant from 273 to 294 K, as shown in Figure 11. We can employ eq 3 to relate values of K_{HCl} at these temperatures if the temperature dependence of D_{HCl} is known. The conductance of Cl^- in pure glycerol varies nearly inversely with viscosity in this temperature range such that $\lambda^\infty_{Cl^-} \sim \eta(T)^{-0.92}$.[15] In contrast, the transference number T_{H^+} varies only weakly in glycerol−water mixtures from 294 to 273 K.[14] These conductance measurements yield a ratio of diffusion coefficients of $D_{HCl}(294\ K)/D_{HCl}(273\ K) = 8.0 \pm 0.3$. Assuming that β and τ do not change over the 21 K interval, the ratio of equilibrium constants $K_{HCl}(294\ K)/K_{HCl}(273\ K)$ is computed to be 0.12 ± 0.02. The HCl enthalpy and entropy of solvation extracted from this ratio are $\Delta H^\circ_{HCl}(gly) = -67 \pm 4$ kJ mol^{-1} and $\Delta S^\circ_{HCl}(gly) = -165 \pm 20$ J mol^{-1} K^{-1}. Despite the uncertainties in this calculation, the −67 kJ mol^{-1} solvation enthalpy is only slightly smaller than calorimetric measurements of ΔH°_{HCl} at 298 K in ethylene glycol (−68 kJ mol^{-1}),[42,44] in 83 mol % glycerol/17 mol % H_2O (−69 kJ mol^{-1}),[45] and in water (−75 kJ mol^{-1}). In addition, the entropy change is similar to the value of $\Delta S^\circ_{HCl} = -170$ J mol^{-1} K^{-1} for HCl dissolution in ethylene glycol but more negative than that in water for which $\Delta S^\circ_{HCl} = -130$ J mol^{-1} K^{-1}.[42,44] Within this analysis, ΔG°_{HCl} is less negative in glycerol than in water because of similar contributions from the lower exothermicity and the greater loss in entropy upon dissolution. This entropy loss may arise from a more extensive ordering of glycerol molecules around H^+ and Cl^- than that occurring in water.

Our information about the thermodynamics of HBr dissolution is more limited than that for HCl. On the basis of an extrapolated residence time of HBr in glycerol of 10 s or longer, an estimated HBr flux of 10^{15} cm^{-2} s^{-1}, and $D_{HBr} \approx D_{HCl}$, we calculate $K_{HBr}(gly)$ to be 10^5 or larger. This value yields $\Delta G^\circ_{HBr} \leq -30$ kJ mol^{-1}, which is at least 10 kJ mol^{-1} more negative than that for the weaker acid HCl.

Summary

The combined uptake, scattering, and D → H exchange measurements demonstrate that HCl and HBr molecules readily dissipate their excess kinetic energy and become momentarily trapped at the surface of glycerol. Nearly all thermalized HBr molecules dissolve in the protic liquid rather than desorb, and they remain in the acid for at least 10 s, most likely as H^+ and Br^-. In contrast, 20% of the thermalized HCl molecules escape reaction by desorbing before they dissociate. HCl molecules that do dissolve in glycerol dissociate fully into ions with exothermicity (−67 kJ mol^{-1}) and entropy losses (−165 J mol^{-1} K^{-1}) that are less favorable than in water but are similar to dissolution in ethylene glycol. The equilibrium constant for $HCl(g) \rightleftharpoons H^+(gly) + Cl^-(gly)$ is measured to be 2300 M^2 atm^{-1} at 294 K, which is 1400 times smaller than the value in water but is large enough to sequester HCl within glycerol for average residence times of 1 to 0.1 s at incident HCl fluxes of 0.2×10^{15} to 2×10^{15} cm^{-2} s^{-1}. DCl scattering experiments indicate that complete $D^+ \rightarrow H^+$ exchange occurs during this time, whereas the inverse flux dependence of the residence time shows that the desorbing HCl molecules are reformed from H^+ and Cl^- originally belonging to two different HCl molecules. In the following paper, we exploit the high solubility, long residence time, and second-order recombination of H^+ and Cl^- in glycerol to identify an unexpected DCl → HCl exchange and desorption pathway that takes place within 10^{-6} s in the near-interfacial region.

Appendix

Extracting the Initial Uptake and Residence Time of HCl from the Observed Uptake. This Appendix outlines the calculation of the uptake and desorption coefficients, $\gamma_{exp}(t)$ and $\gamma_{des}(t)$, that are used in eq 1 to determine the initial uptake probability $\beta(E_{inc}, \theta_{inc})$ and the residence time τ from the measured gas uptake γ_{obs}. The coefficients are computed by solving the mass conservation equations for HCl across the boundary at $x = 0$ separating the gas and liquid for the beam-on region at $0 < t < t_{exp}$:

$$-D\, \partial c_l(x, t)/\partial x|_{x=0} = F_{in} - F_{des}(t) \equiv \gamma_{exp}(t)\, F_{beam} \qquad (A.1)$$

and for the beam-off region at $t_{exp} < t < t_{des} + t_{exp}$

$$-D\, \partial c_l(x, t)/\partial x|_{x=0} = -F_{des}(t) \equiv -\gamma_{des}(t)\, F_{beam}$$

The liquid-phase diffusion coefficient and concentration of HCl in the glycerol film are D and $c_l(x, t)$, respectively, where $x =$

0 is the boundary separating gas and liquid and the impinging flux is F_{beam}. The beam-on and beam-off regions are depicted in Figure 2. The flux of HCl entering the liquid as molecular HCl or as $H^+ + Cl^-$ after first dissociating in the interfacial region is equal to $F_{in} = \beta(E_{inc}, \theta_{inc})\, F_{beam}$. $F_{des}(t)$ is the time-dependent flux of molecules leaving the liquid such that $F_{des}(t) = 0$ at $t = 0$ and $F_{des}(t) \rightarrow F_{in}$ at $t \rightarrow \infty$.

The impinging and desorbing fluxes can be expressed in terms of gas- and liquid-phase concentrations

$$\beta(E_{inc}, \theta_{inc})\, F_{beam} = F_{in} = \beta_{th} \nu_{th} c_g^*/4 = \beta_{th} \nu_{th} c_l^{*2}/[4RTK_{HCl}] \quad (A.2)$$

and

$$F_{des}(t) = \beta_{th} \nu_{th} c_g(t)/4 = \beta_{th} \nu_{th} c_l(x = 0, t)^2/[4RTK_{HCl}]$$

where c_g^* is the effective HCl concentration in an effusive beam whose flux into the liquid, $\beta_{th} \nu_{th} c_g^*/4$, is set equal to F_{in}. At saturation, the concentration of H^+ and Cl^- in the liquid phase is given by $K_{HCl} = c_l^{*2}/P_g$, and $P_g = c_g^* RT$ for the reaction $HCl(g) \rightleftharpoons H^+(gly) + Cl^-(gly)$. $F_{des}(t)$ is expressed in terms of $c_g(t)$, which is the gas-phase concentration of HCl molecules leaving the liquid at time t and is the concentration that would be in equilibrium with a liquid-phase concentration equal to $c_l(x = 0, t)$.[46]

By combining eqs A.1 and A.2, we construct expressions in terms of $c_l(x = 0, t)$ for the uptake and desorption coefficients in the beam-on region

$$\gamma_{exp}(t) = \beta(E_{inc}, \theta_{inc})[1 - c_l^2(x = 0, t)/c_l^{*2}] \quad (A.3)$$

and the beam-off region

$$\gamma_{des}(t) = \beta(E_{inc}, \theta_{inc})[c_l^2(x = 0, t)/c_l^{*2}]$$

and for the boundary conditions in the beam-on and beam-off regions

$$-D\, \partial[c_l(x, t)/c_l^*]/\partial x|_{x=0} = (D/\tau)^{1/2}(1 - c_l^2(x = 0, t)/c_l^{*2}) \quad \text{beam-on}$$

$$= -(D/\tau)^{1/2} c_l^2(x = 0, t)/c_l^{*2} \quad \text{beam-off} \quad (A.4)$$

The values of $c_l(x = 0, t)/c_l^*$ are found by numerical solution[47] of the diffusion equation, $D\, \partial^2[c_l(x, t)/c_l^*]/\partial x^2 = \partial[c_l(x, t)/c_l^*]/\partial t$, using the boundary conditions A.4. The ratio $c_l(x = 0, t)/c_l^*$ depends on τ, given by eq 2, but not on D. Equation A.4 is quadratic in $c_l(x = 0, t)/c_l^*$ and is linearized by substituting $c_l(t)\, c_l(t - \Delta t)$ for $c_l(t)\, c_l(t)$ in the numerical solution using time steps of $\Delta t/t_{exp}$ typically less than 0.005. $\beta(E_{inc}, \theta_{inc})$ and τ are obtained by trial and error and by using eq 1 to construct a best-fit line through the graph of γ_{obs} versus t_{exp}.

Figure A.1 illustrates the shapes of $\gamma_{exp}(t)$ and $\gamma_{des}(t)$ for $\theta_{inc} = 45°$ and $t_{exp}/t_{des} = 0.5$ for $\tau = 0.4$ s. The net uptake drops between $t = 0$ and t_{exp} as molecules initially dissolved in the glycerol begin to desorb. For longer solvation times τ, the uptake would change more slowly with t_{exp}. In the beam-off region, the rate of gas desorption is initially high but declines as the liquid is depleted of HCl. The inset shows the liquid-phase profiles of the solute at $t = t_{exp}$ and at $t = t_{exp} + t_{des}/2$ (the time halfway through the desorption region), illustrating the depletion of solute near the surface because of desorption. When HCl does not dissociate, when H^+ is in excess, or for recombination

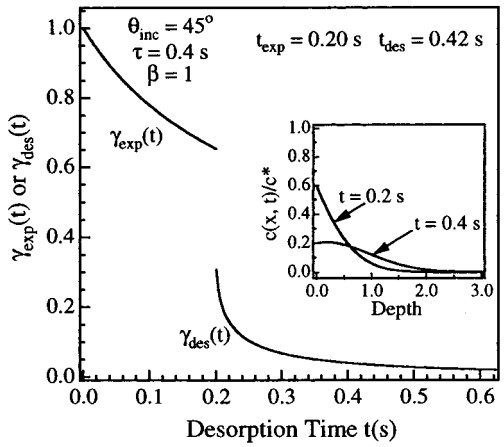

Figure A.1. Uptake and desorption coefficients, $\gamma_{exp}(t)$ and $\gamma_{des}(t)$, versus desorption time t for $\beta = 1$ and $\tau = 0.4$ s for a molecule HX that dissociates in solution. The transition from the beam-on to the beam-off region occurs at 0.2 s. The inset shows the relative concentration profiles of X^- or H^+ in the liquid at 0.2 and 0.4 s.

of $H^+ \cdot Cl^-$ ion pairs, $\gamma_{exp}(t) = \beta(E_{inc}, \theta_{inc})[1 - c_l(x = 0, t)/c_l^*]$ and is linear in c_l. This equation can be expressed as $\gamma_{exp}(t) = \beta(E_{inc}, \theta_{inc})\, \mathrm{erfc}((t/\tau)^{1/2})\, \exp(t/\tau)$. The ratio $\gamma_{exp}(\tau)/\gamma_{exp}(0)$ is 0.43 for the linear case and 0.48 for the quadratic case.

We note that eqs 2 and 3 determine the HCl solvation time τ even when the molecules are delivered to the surface by a nonthermal supersonic beam. This situation occurs because molecules that are trapped at the surface and then dissolve in the liquid lose the memory of their initial trajectory, allowing the incident flux to be expressed in terms of an effective effusive flux, given by eq A.2.

Residence Times from Post-Chopper Spectra. Approximate values of τ can be extracted from the integrated TD components of the TOF spectra for D → H-exchanged HCl. At $\theta_{inc} = \theta_{fin} = 45°$, the mass spectrometer images an area slightly larger than the beam spot, so only desorption in the beam-on region is observed. The desorption probability, $p_{des}(t) = F_{des}(t)/F_{des}(t \rightarrow \infty)$, is equal to $c_l^2(x = 0, t)/c_l^{*2}$. The ratio of concentrations depends on τ but not on β. The residence time is calculated from

$$I_{TD}(t_{exp})/I_{TD}(t_{exp}') = [(1/t_{exp})\int_0^{t_{exp}} p_{des}(t)\, dt]/[(1/t_{exp}')\int_0^{t_{exp}'} p_{des}(t)\, dt] \quad (A.5)$$

Before using eq A.5, the intensities are corrected by removing the component due to immediate exchange and desorption, as discussed in the following paper. For the data in Figure 6a, the intensity ratio $I_{TD}(0.45\ s)/I_{TD}(0.045\ s)$ is 0.42 before correction and 0.23 after correction. This value is best fit using eq A.5 with $\tau = 0.17 \pm 0.05$ s.

Acknowledgment. We are grateful to the National Science Foundation for supporting this work. We also thank Professor Edwin Sibert, Professor Arun Yethiraj, and Dr. Qu Shi for advice on numerical analysis of the gas uptake data.

References and Notes

(1) Miner, C. S. *Glycerol*; Reinhold Publishing Corporation: New York, 1953.
(2) Newman, A. A. *Glycerol*; C. R. C. Press: Cleveland, OH, 1968.
(3) Root, L. J.; Stillinger, F. H. *J. Chem. Phys.* **1988**, *90*, 1200.
(4) Commenga, H. K.; Schulze, F. W.; Thuerl, W. *J. Chem. Eng. Data* **1977**, *22*, 131.
(5) Bastos, M.; Nilsson, S.; Riberio Da Silva, M. D.; Riberio Da Silva, M. A.; Wadso, I. *J. Chem. Thermodyn.* **1988**, *20*, 1353.

(6) Saecker, M. E.; Nathanson, G. M. *J. Chem. Phys.* **1993**, *99*, 7056.
(7) Bohmer, R.; Ngai, K. L.; Angell, C. A.; Plazek, D. J. *J. Chem. Phys.* **1993**, *99*, 4201.
(8) Champeney, D. C.; Kaddour, F. O. *Mol. Phys.* **1984**, *52*, 509.
(9) Benjamin, I.; Wilson, M. A.; Pohorille, A. *J. Chem. Phys.* **1994**, *100*, 6500.
(10) Benjamin, I.; Wilson, M. A.; Pohorille, A.; Nathanson, G. M. *Chem. Phys. Lett.* **1995**, *243*, 222.
(11) Baldelli, S.; Schnitzer, C.; Shultz, M. J.; Campbell, D. J. *J. Phys. Chem. B* **1997**, *101*, 4607.
(12) Tassotto, M.; Gannon, T. J.; Watson, P. R. *J. Chem. Phys.* **1997**, *107*, 8899.
(13) Good, R. J. *J. Phys. Chem.* **1957**, *61*, 810.
(14) Erdey-Gruz, T.; Majthenyi, L.; Nagy-Czako, I. *Acta Chim. Acad. Sci. Hung.* **1967**, *53*, 29.
(15) Hammadi, A.; Champeney, D. C. *J. Chem. Eng. Data* **2000**, *45*, 1116.
(16) Morris, J. M.; Behr, P. M.; Antman, M. D.; Ringeisen, B. R.; Splan, J.; Nathanson, G. M. *J. Phys. Chem. A* **2000**, *104*, 6738.
(17) Lednovich, S. L.; Fenn, J. B. *AIChE J.* **1977**, *23*, 454.
(18) King, D. A.; Wells, M. G. *Proc. R. Soc. London, Ser. A* **1974**, *339*, 245.
(19) Fiehrer, K. M.; Nathanson, G. M. *J. Am. Chem. Soc.* **1997**, *119*, 251.
(20) Hanson, D. R. *J. Phys. Chem. B* **1997**, *101*, 4998.
(21) Shi, Q.; Davidovits, P.; Jayne, J. T.; Worsnop, D. W.; Kolb, C. E. *J. Phys. Chem. A* **1999**, *103*, 8812.
(22) Ringeisen, B. R. Ph.D. Thesis, University of Wisconsin, 1999.
(23) The variations in γ_{obs}(HBr) with exposure time at $\theta_{inc} = 45°$ were scaled from measurements at different t_{exp} at $\theta_{inc} = 0°$.
(24) Kroes, G.-J.; Clary, D. C. *J. Phys. Chem.* **1992**, *96*, 7079.
(25) Hurst, J. E.; Becker, C. A.; Cowin, J. P.; Janda, K. C.; Wharton, L.; Auerbach, D. J. *Phys. Rev. Lett.* **1979**, *43*, 1175.
(26) Harris, J. In *Dynamics of Gas−Surface Interactions*; Rettner, C. T., Ashfold, M. N. R., Eds.; Royal Society of Chemistry: Cambridge, 1991.
(27) Bolton, K.; Svanberg, M.; Pettersson, J. B. C. *J. Chem. Phys.* **1999**, *110*, 5380.
(28) Andersson, P. U.; Nagard, M. B.; Pettersson, J. B. C. *J. Phys. Chem. B* **2000**, *104*, 1596.
(29) Klassen, J. K.; Fiehrer, K. M.; Nathanson, G. M. *J. Phys. Chem. B* **1997**, *101*, 9098.
(30) The prechopper measurements described in the next paper show that the Ar residence times are shorter than 10^{-6} s.
(31) Grimmelmann, E. K.; Tully, J. C.; Cardillo, M. J. *J. Chem. Phys.* **1980**, *72*, 1039.
(32) Rieley, H.; Aslin, H. D.; Haq, S. *J. Chem. Soc., Faraday Trans.* **1995**, *91*, 2349.
(33) Isakson, M. J.; Sitz, G. O. *J. Phys. Chem. A* **1999**, *103*, 2044.
(34) For trapping of H_2O on water ice, see Brown, D. E.; George, S. M.; Huang, E. K.; Wong, E. K. L.; Rider, K. B.; Smith, R. S.; Kay, B. D. *J. Phys. Chem.* **1996**, *100*, 4998. For trapping of D_2O and CH_3CH_2OH on azeotropic sulfuric acid, see ref 19 and Govoni, S. T.; Nathanson, G. M. *J. Am. Chem. Soc.* **1994**, *116*, 779.
(35) Graham, J. D.; Roberts, J. T. *J. Phys. Chem.* **1994**, *98*, 5974.
(36) Van Doren, J. M.; Watson, L. R.; Davidovits, P.; Worsnop, D. R.; Zahniser, M. S.; Kolb, C. E. *J. Phys. Chem.* **1990**, *94*, 3265. Li, Y. Q.; Zhang, H. Z.; Davidovits, P.; Jayne, J. T.; Kolb, C. E.; Worsnop, D. R. *J. Phys. Chem. B.* **2002**, *106*, 1220.
(37) Schwitzer, F.; Mirabel, P.; George, C. *J. Phys. Chem. A* **2000**, *104*, 72.
(38) As shown later, the near-interfacial concentration of HCl should not exceed 0.01 M at the highest HCl flux. The highest steady-state ratio of HCl to glycerol at the surface is therefore close to 0.01 M/13 M or ∼0.1%. This small ratio indicates that HCl molecules already at the surface should not interfere with the adsorption of incoming HCl.
(39) As discussed later, $D_{Cl^-} \approx 5 \times 10^{-8}$ cm^2 s^{-1}, and the transference number $T_{H^+} \geq 0.93$, which yields $D_{H^+} \geq 5 \times 10^{-7}$ cm^2 s^{-1} and a summed diffusion coefficient of at least this value.
(40) For a dilute ionic solution, $R_{ion} = a/(1 - e^{-r/R})$ where $a = e^2/(4\pi\epsilon_o\epsilon k_B T)$, $R \approx 4$ Å is the distance of closest approach, and $\epsilon = 41$. At 294 K, $R_{ion} = 14$ Å but should be reduced slightly because of screening from nearby ions at [HCl] = 10^{-3} M. See Amdur, I.; Hammes, G. G. *Chemical Kinetics*; McGraw-Hill: New York, 1966; p 59.
(41) For KCl, the ion activity coefficient $f_\pm$ decreases from 0.92 at 0.001 M to 0.78 at 0.010 M in glycerol (see Champeney, D. C.; Comert, H. *Phys. Chem. Liq.* **2000**, *18*, 43). A drop in $f_\pm$ at higher HCl flux would limit $P_{HCl}(t) = f_\pm^2[Cl^-(t)]^2/K_{HCl}$ and suppress the time-dependent HCl desorption flux, lengthening τ more than predicted by eq 4, as observed in Figure 9.
(42) Stern, J. H.; Nobilione, J. M. *J. Phys. Chem.* **1968**, *72*, 3937.
(43) Carslaw, K. S.; Clegg, S. L.; Brimblecombe, P. *J. Phys. Chem.* **1995**, *99*, 11557.
(44) Elsemongy, M. Â. *Thermochim. Acta* **1986**, *103*, 387.
(45) Stern, J. H.; Hansen, S. L. *J. Phys. Chem.* **1981**, *85*, 3713.
(46) Danckwerts, P. V. *Gas−Liquid Reactions*; McGraw-Hill: New York, 1970.
(47) Press, W. H.; Teukolsky, S. A.; Vetterling, W. T.; Flannery, B. P. *Numerical Recipes in FORTRAN*; Cambridge University Press: New York, 1992; pp 838−842.